

The Nature of Surface Oxides on Corrosion-Resistant Nickel Alloy Covered by Alkaline Water

Jiaying Cai · D. F. Gervasio

Received: 16 November 2009 / Accepted: 17 December 2009 / Published online: 5 January 2010
© The Author(s) 2010. This article is published with open access at Springerlink.com

Abstract A nickel alloy with high chrome and molybdenum content was found to form a highly resistive and passive oxide layer. The donor density and mobility of ions in the oxide layer has been determined as a function of the electrical potential when alkaline water layers are on the alloy surface in order to account for the relative inertness of the nickel alloy in corrosive environments.

Keywords EIS · Mott–Schottky · Bipolar plates · High-temperature PEM fuel cell · Nickel alloy

Introduction

Nickel metal alloys are corrosion resistant and can serve as structural materials in extraordinary environments, e.g., in long-term storage containers, high-temperature heat exchangers and aggressive chemical reactors. The stability is often attributed to the inertness of the oxides that form on the nickel alloys. One new application of these extraordinary alloys is as the structural material for a metal bipolar plate in a polymer electrolyte membrane (PEM) fuel cell stack.

The bipolar plate is among the most expensive, heaviest and voluminous components in the fuel cell stack. The bipolar plates conduct current between cells, provide flow channels for reactants and products, facilitate water and

thermal management and constitute the structural backbone of a fuel cell stack. The materials for bipolar plates need to have high electric and thermal conductivity, good corrosion resistance and mechanical strength. Replacing bulky, brittle machined graphite plates by thin, durable stamped metal plates is particularly desirable for portable and mobile applications where lower bulk, fragility and cost are all needed.

After an earlier accelerated corrosion screening test [1], the high chrome molybdenum nickel alloys, such as Hastelloy C22 (composition given in Table 1), were considered one of the few materials with structural stability that is suitable for use in bipolar plates for a high-temperature PEM fuel cell stack.

Compared with graphite, C22 can be made into bipolar plates from much thinner sheets. The thickness of a C22 metal sheet is <0.1 mm, whereas that of a graphite sheet is >2–5 mm. The C22 can be formed into a bipolar plate by a lower cost stamping as the manufacturing method, which costs only 10 cents to \$1 per plate when compared to \$5–\$25 per plate for the milling or molding a graphite plate [2]. These features of metal bipolar plates are desirable for making a more compact, lighter weight and lower cost fuel cell stack.

Most importantly, alloy C22 shows remarkable corrosion resistance and stability that is suitable in the aggressive fuel cell environment. A number of studies on its general and local corrosion resistance suggest that C22 has excellent resistivity in a broad range of concentrated brines including chloride, fluoride, carbonate, sodium and calcium over a large pH and temperature range [3]. It is mainly due to the formation of a protective passive oxide layer on the surface. This occurs through electrochemical “local cell” on the metal surface, where oxygen reduction occurs at one localized metal surface site by accepting electrons

J. Cai (✉)
Department of Chemical Engineering, Arizona State University,
Tempe, AZ, USA
e-mail: jiaying.cai@asu.edu

D. F. Gervasio
Department of Chemical Engineering, University of Arizona,
Tucson, AZ, USA

Table 1 Chemical composition (wt%) of Alloy C22

	Co	Cr	Fe	Mn	Mo	Ni	P	S	Si	V	W
C22	1.45	15.74	5.58	0.50	15.53	57.55	0.008	0.003	0.02	0.163	3.54

generated during metal oxidation occurring at another localized site through electron conduction in the bulk metal [4]. The oxygen reduction site becomes alkaline, and metal oxidation site becomes acidic. Nickel alloy was placed in aqueous potassium hydroxide solution and exposed to various oxidizing potentials representative of a bipolar plate at an oxygen cathode. Electrochemical impedance spectroscopic (EIS) and Mott–Schottky (M–S) methods were used to determine the density and mobility of charge carriers in the passive oxide layer to understand the nature of the surface oxides and how these affect the corrosion resistance of C22 nickel alloy covered by alkaline water.

Experimental

Electrochemical Measurements

All electrochemical experiments were carried out using a three-electrode configuration at room temperature. The working electrode was nickel alloy C22 (Haynes), machined into 6 cm × 2 cm × 0.2 cm. The working electrode was abraded with 1200-grit SiC paper, polished with 1.0, 0.3 and 0.05 μm Al₂O₃ powder and then ultrasonically cleaned in deionized water. The working electrode area was 12 cm². A Ag/Ag₂O reference electrode was used in 0.1 M KOH (pH 13.0) and in 1.0 M KOH (pH 13.8) electrolyte solution. The potential of the silver/silver-oxide reference electrode is 0.321 V versus RHE in 0.1 M KOH and 0.341 V versus RHE in 1.0 M KOH. This can be related to NHE (pH = 0) by the potential shift with pH using the Nernst equation. A graphite rod was used as the counter electrode. The aqueous alkaline potassium hydroxide solutions of two concentrations (0.1 M, pH 13.0 and 1.0 M, pH 13.8) were prepared using pure deionized water (PureLab Ultra system) and potassium hydroxide stock (analytical-grade reagent). The solution was deaerated with ultrapure nitrogen gas for 30 min prior to starting the experiment, and this nitrogen purge was continued throughout each experiment. Voltammetry of Alloy C22 was performed to determine the electrochemical processes that occur on the moisture-covered alloy surface. After freshly abrading the C22 working electrode, it was cathodically polarized at −1.3 V for at least 20 min to remove the air-formed oxide film, then the potential was swept from −1.3 to 0.5 V at a scan rate of 20 mV/s to survey the surface processes. The C22-alloy working

electrode was held for 2 h at each film formation potential to grow the passive oxide films.

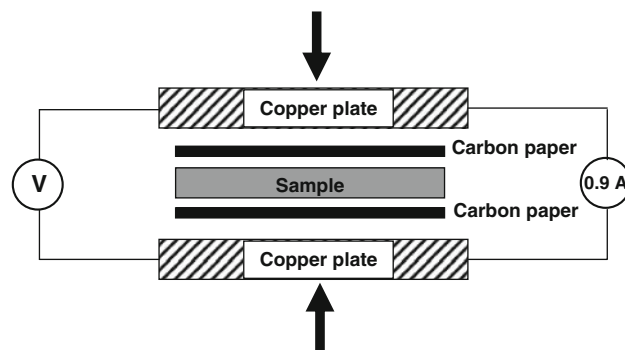
EIS and M–S tests were carried out immediately after the passive films were formed. For EIS measurements, the frequency was analyzed over a range of 10 kHz–1 MHz with a peak-to-peak modulation amplitude voltage of 20 mV. And then, the M–S experiments were done by measuring the frequency at 1 kHz during a negative potential scan from +0.2 to −1.1 V in 50 mV-increments.

All electrochemical experiments were performed using a Princeton Applied Research VMP2/Z Multichannel Potentiostat (Oak Ridge, TN) running EC-Lab version 9.13 software, and the impedance spectra analyses were performed using Zsimpwin software.

Interfacial Contact Resistance (ICR)

ICR should be minimized for bipolar plates to achieve high efficiency in PEM fuel cells. ICR measurement was conducted on the Hastelloy C22 after the electrochemical oxidization. The apparatus for measuring ICR is illustrated in Fig. 1, showing two pieces of carbon paper (SIGRACET, type GDL 10 AA, a gas diffusion layer used in PEM fuel cells) sandwiched between the sample and two copper plates. Compaction force was applied by a hydraulic press. The potential difference *V* across the cell and the copper plates was measured by an ohmmeter while a fixed electrical current *I* (0.9 A) was passed through the arrangement. The ICR was calculated as follows [5]:

$$\text{ICR} = \frac{R - R_{cp}}{2} \times A$$

**Fig. 1** Apparatus used to measure interfacial contact resistance

where R is the total resistance (V/I), R_{cp} represents the resistant contribution due to the carbon paper/copper plates ($\sim 5 \text{ m}\Omega$) and A is the sample area (cm^2). The value of ICR was greatly affected by the compaction force, and good reproducibility could be obtained only with compaction force above 200 N cm^{-2} [5, 6].

Auger Electron Spectroscopy (AES)

In order to determine the general composition of surface-oxidized C22, AES was performed to get depth profile for oxidized samples. AES analyses were carried out on specimens at sputter rate of 2.0 nm per minute with beam current of $1.0 \mu\text{A}$ and beam voltage of 4.0 kV using Physical Electronics 590 Scanning Auger Microprobe.

Results and Discussion

Cyclic Voltammetry

The cyclic voltammogram presented in Fig. 2 shows the surface processes occurring on alloy C22 in both 0.1 M (pH 13.0) and 1.0 M KOH (pH 13.8) solution. Figure 2a shows that the first cycle was noticeably different than the successive cycles. The first positive-going sweep shows extra anodic current from -0.7 to 0.3 V , suggesting the formation of a metal oxide layer on the alloy C22 surface. The reverse scan showed the reduction peak between 0.1 and 0.3 V in the first and succeeding negative-going scans. The second and successive positive- and negative-going scans showed growing oxidation and reduction peaks. After the third cycle, the growth rate of both oxidation and reduction peaks decreased and were virtually stable. Figure 2b shows a similar behavior for the cyclic

voltammogram of the C22 in 1.0 M KOH, except there are two noticeable differences. First, there is a slight shift for the anodic peak, which was 0.3 V (vs. $\text{Ag}/\text{Ag}_2\text{O}/0.1 \text{ M KOH}$) for 0.1 M KOH and 0.26 V (vs. $\text{Ag}/\text{Ag}_2\text{O}/1.0 \text{ M KOH}$) for 1.0 M KOH solutions. Secondly, both the oxidation and reduction peak currents were about two times larger in the solution with 1 M versus 0.1 M KOH.

Interfacial Contact Resistance (ICR)

Figure 3 shows the comparison of the ICR of the alloy oxidized at different potentials in both 1.0 M KOH (pH 13.8) and 0.1 M KOH (pH 13.0) solutions. The results showed that the alloy oxidized in 0.1 M KOH had a higher ICR value than that in 1.0 M KOH solution. In both solutions, the ICR values were higher in the passive region (-0.5 to -0.1 V) and decreased at the higher potential conditions.

Generally, the influence of Cr-oxide on the Ni-based material resistance is very complex, and it can be considered

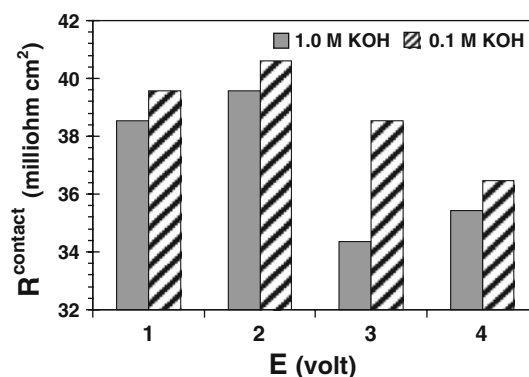


Fig. 3 Interfacial contact resistance of alloy C22 after oxidized at -0.5 , -0.1 , 0.1 and 0.2 V in 1.0 and 0.1-M KOH solutions

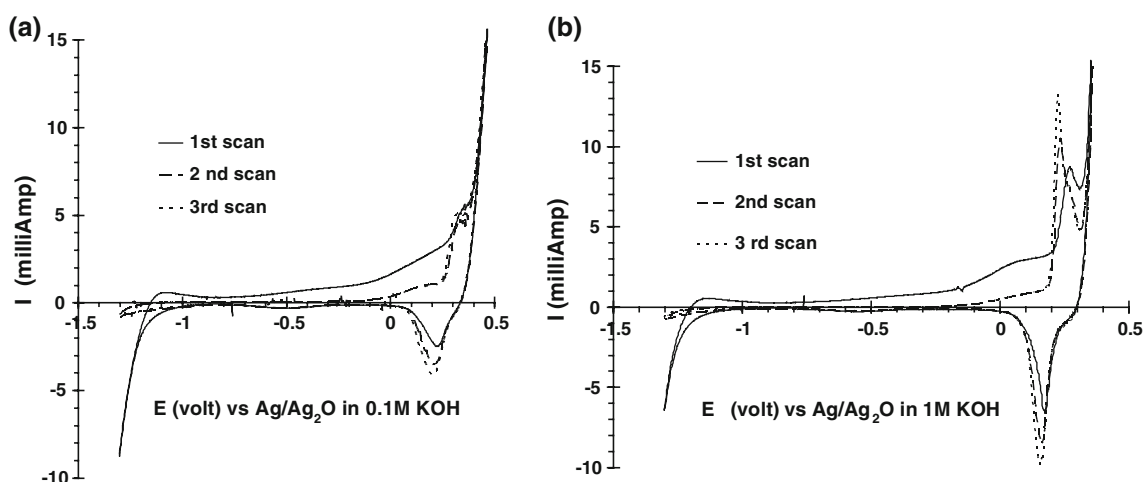


Fig. 2 a, b CV of C22 in 0.1 M and 1.0 M KOH

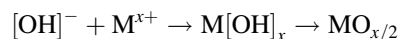
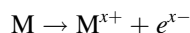
that the decrease of conductivity follows the trend that the conductivity of Ni-oxide is greater than the conductivity of Cr-oxide [5]. Therefore, it appears that when alloy C22 is oxidized in 0.1 M KOH solution, a larger amount of Cr-oxide forms on the surface, which results in a higher value of ICR. The depth profile for the oxide films on C22 by AES (not shown here) showed more Cr-oxide was formed in 0.1 M KOH, which is consistent with this assertion.

Impedance Measurement

EIS and M–S tests were carried out on the passive films formed at different potentials in order to investigate the influence of the film formation potential on the character of passive films on alloy C22. The Nyquist plots are shown in Fig. 4a and c for the nickel alloy in 1.0 and 0.1 M KOH electrolyte. The impedance data can be modeled by a simple equivalent circuit R_s ($C_{sc}Rp$), where R_s is the electrolyte solution resistance, C_{sc} is the space charge capacity and R_p is the polarization resistance. It is clear that the impedance response is sensitive to the film formation potential. In both 0.1- and 1-M KOH solutions, smaller arcs were observed in the potential range of 0.2 and 0.4 V, while larger ascending arcs, which do not form semicircles on the real axis, are observed between -0.3 and -0.1 V. This phenomenon is more clearly shown in Fig. 4b and d, where R_p initially increased with potentials

(within the passive range), but when potentials are within the trans-passive region ($E > -0.1$ V), R_p decreases with E . The existence of the resistance R_p versus E peak can be attributed to the establishment of passive oxide layer in the beginning and then the oxidative ejection of chromium cations from the barrier oxide layer [7].

The impedance behavior for alloy C22 in the 0.1- and 1-M KOH solutions show one systematic difference, namely, the arcs are always larger in 0.1 M KOH. It appears that the higher concentration of $[OH]^-$ ions results in a less-resistive passive oxide film on the nickel alloy surface, especially in the potential range between -0.5 and -0.1 V. The possible formation process of metal oxide is presented as follows.



Having more $[OH]^-$ ions in solution favors the above reaction, and hence, the quick formation of an passive oxide layer, which covers the metal surface and slowed down the further oxidization of metal.

Following each EIS measurement, an M–S test was performed to study the semiconducting properties of a passive oxide film that was formed on the surface of the nickel alloy. The M–S analysis measures the electrode capacitance as a function of potential. Under depletion conditions, the M–S relationship is given by Eq. (1)

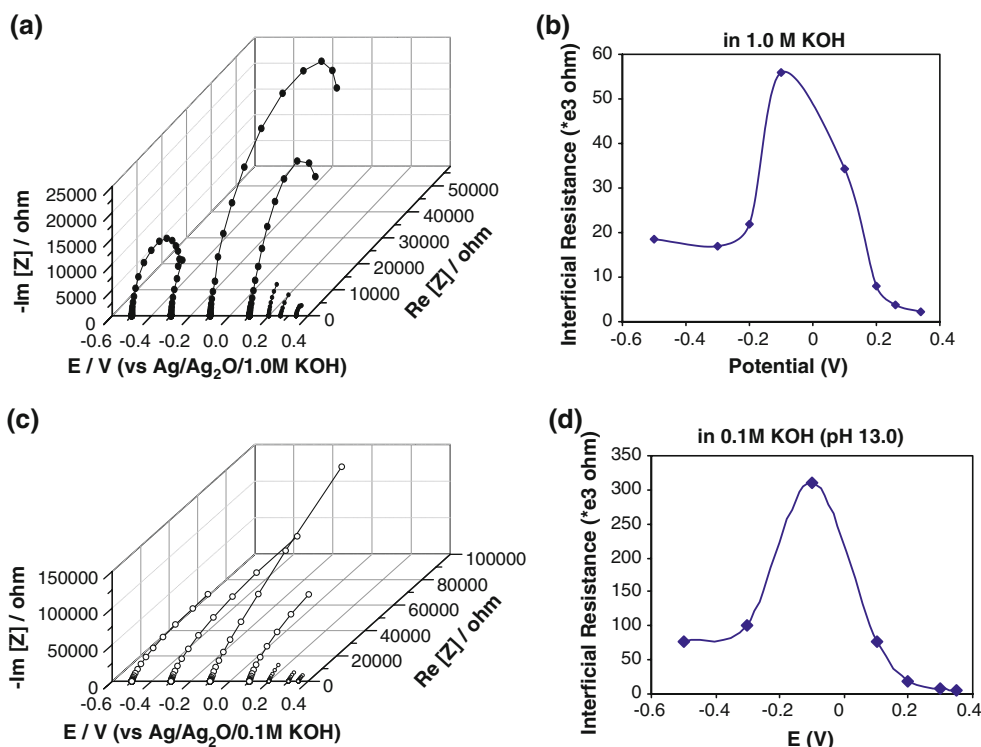


Fig. 4 a, b EIS of C22 in 1.0 M KOH. c, d EIS of C22 in 0.1 M KOH

$$\frac{1}{C_{SC}^2} = \frac{2}{e\epsilon\epsilon_0NA^2} \left(V_E - V_{fb} - \frac{kT}{e} \right) \tag{1}$$

where C_{SC} is the space charge capacitance, ϵ is the dielectric constant of the semiconductor, ϵ_0 is permittivity of free space ($8.854e^{-14}$ F/cm), N is defect density (electron donor concentration for n-type semiconductor or hole acceptor concentration for p-type semiconductor) and k is the Boltzmann constant. kT/e is the thermal voltage, which is the voltage a single charge falls through to pick up the thermal energy. kT/e is about 25 mV at the ambient temperature.

The M–S analysis assumes the space charge capacitance is much smaller than the double-layer capacitance such that the contribution of double-layer capacitance to the total capacitance value could be negligible. For a p-type semiconductor, C_{SC}^{-2} versus E should be linear with a negative slope, which is inversely proportional to the acceptor density N . For an n-type semiconductor, the slope should be positive.

Figure 5 shows the M–S plots recorded at 1 kHz frequency for passive films formed on Alloy C22 in 1.0- and 0.1-M KOH solutions at different potentials.

As shown in Fig. 5b, the capacitance decreased (C_{SC}^{-2} increased) at low potentials ($-1.1 < E < -0.8$ V), suggesting an n-type semiconductor. At higher potentials

($E > -0.1$ V), however, the capacitance increased (C_{SC}^{-2} decreased), showing a p-type semiconductor. The change of the electronic character is more likely due to the generation of the cation vacancies at film/solution interface through the oxidative ejection of cations from the film [8]. This result is consistent with the above Nyquist plots where the most resistant film was formed at the potential of -0.1 V, where the change of electronic character appeared.

Over the potential range between -0.8 and -0.1 V, the capacitance was nearly constant, for those passive films formed at lower potentials ($-0.5, -0.3, -0.2, -0.1$ and 0.1 V). This phenomenon was also reported by Da Belo et al. [9] on Ni-20% Cr alloy in pH 9.2 borate buffer. For those passive films formed at higher potentials ($0.2, 0.26$ and 0.34 V), there was no clear potential range over which the capacitance varies slightly. Their M–S profiles behaved similar to those of the films on pure Cr, which presents a peak in the C_{SC}^{-2} versus E plots followed by a steadily linear region negative slope (see [10]).

Defect density N of the passive films could also be determined by the slope of the linear part of M–S profile. Both the donor density calculated from the n-type part and the acceptor density from the p-type part in passive films formed in 1.0-M KOH electrolyte solution are larger than those formed in 0.1-M KOH solution (see Fig. 6). The

Fig. 5 a, b M–S test of C22 in 1.0 and 0.1 M KOH

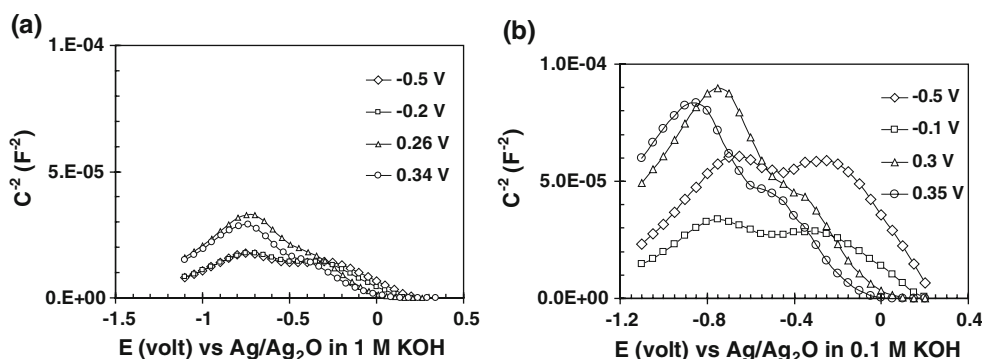
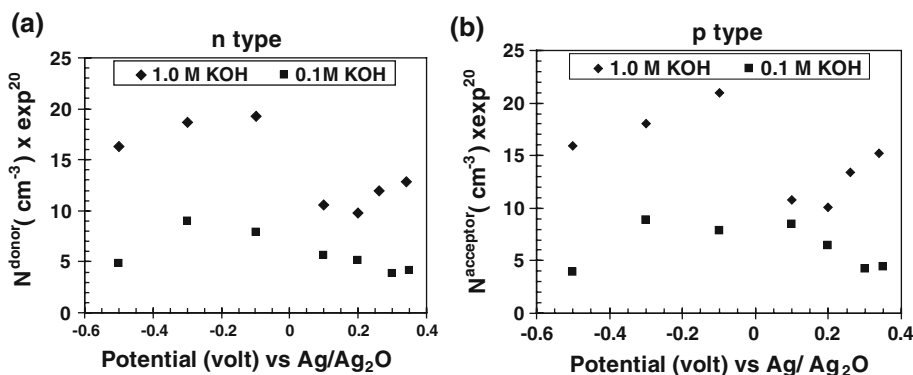


Fig. 6 a, b Donor density (acceptor density) versus film formation potentials



higher defects concentration within the film resulted in lower resistant passive films, and accordingly, higher conductivity, which was in a good agreement with the ICR and Nyquist results.

AES Depth Profile

Figure 7 showed the content of three major components within the surface oxide films on alloy C22 versus the depth of the films.

In all cases, the amount of Cr-oxide was slightly higher in 0.1-M KOH than that in 1.0-M KOH solution. This result is consistent with the effect of solution pH on the ICR value, which was higher for the oxide films formed in 0.1 M KOH.

The depth profile (b) behaved quite different from the other two cases. For the oxide film formed at -0.1 V, the content of Cr-oxide is higher in the outer layer of the film, which was $\sim 51\%$ formed in 1.0 M KOH and $\sim 55\%$ in 0.1 M KOH compared with $\sim 20\%$ in the bulk alloy. It decreased greatly from the outer to inner surface at the depth of 2 nm, while the content of Ni-oxide increased and finally dominated in the inner layer of the film. However, for the oxide films formed at -0.5 and 0.26 V, this dual-layered structure was not observed. And the Ni-oxides were dominant through the entire oxide film. This result could also be explained the highest value of ICR for the oxide film formed at -0.1 V, which the higher amount of Cr-oxide was responsible for the higher contact resistance. The thickness of the oxide films was estimated by the depth profile at the range of 3–4 nm, where the three components Cr, Ni and Mo converged to a state value, respectively.

Conclusions

The oxide film that forms on nickel alloy C22 is affected by film formation potential and pH. ICR and EIS show the interfacial film resistance R_p is sensitive to the film formation potential. The current for the formation of oxide peaks at the potential of -0.1 V. More concentrated KOH electrolyte solution contributes to the formation of less resistant and hence larger peak current for this passive film formation at 0.1 V on nickel alloy C22. The M–S analysis of the oxide layer on nickel alloy C22 shows that the oxide film on the nickel alloy is semiconducting when formed in both 0.1- and 1-M KOH solutions. Over lower potential range, the oxide film on nickel alloy C22 displays n-type character, while p-type character is found at higher potentials. Defect concentration obtained from the M–S plots is higher when the film is formed in 1.0-M KOH solution at all the investigated film formation potentials, which is consistent with a lower film resistance for oxides

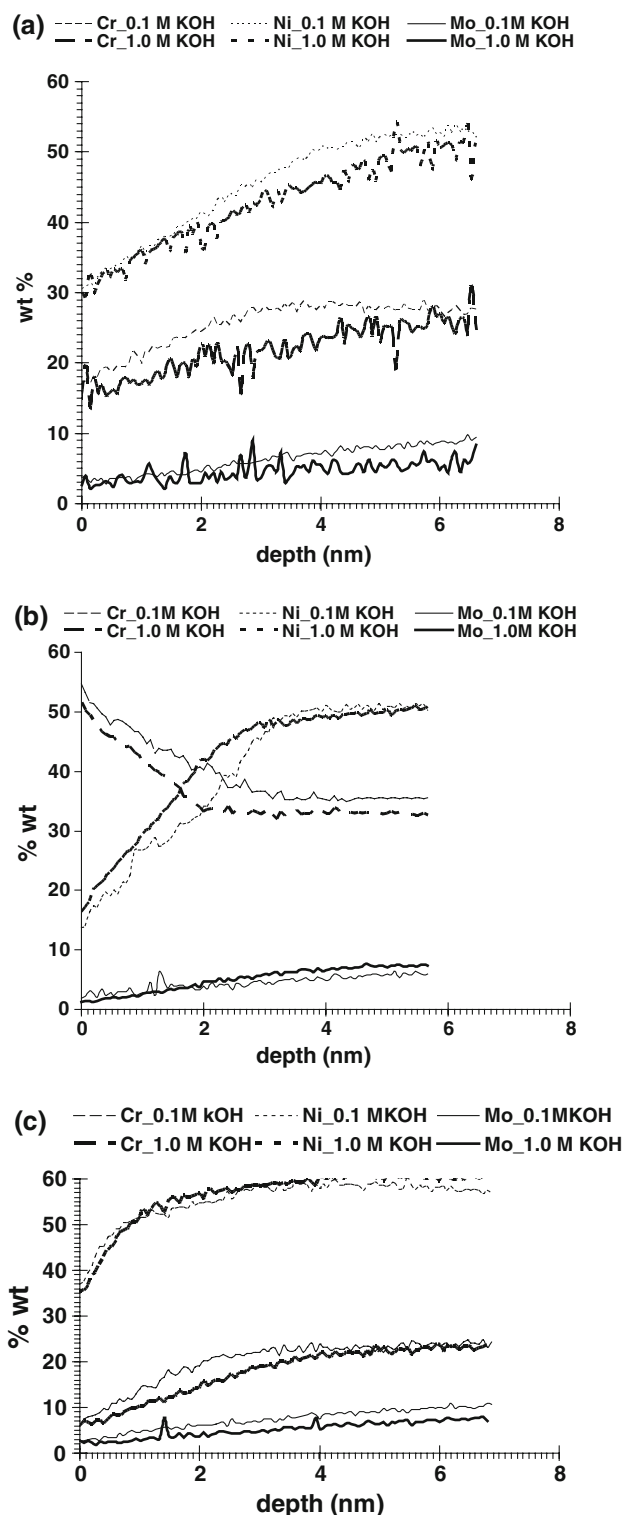


Fig. 7 AES depth profile of the oxide film on alloy C22 formed at -0.5 V (a), -0.1 V (b) and 0.26 V (c) in 0.1 and 1.0 M KOH

formed in 1-M compared to 0.1-M KOH solution. The AES depth profile shows a dual-layered structure in the oxide film formed at -0.1 V, where a Cr-rich outer layer is responsible for the higher contact resistance. The amount

of Cr showed in the depth profile was higher in 0.1-M KOH than that in 1.0-M KOH solution, which further confirmed that a more resistive oxide film grows on the nickel alloy when it is covered by a less concentrated aqueous KOH (less basic) solution.

As is, this alloy is stable enough to be used as a bipolar plate in a high-temperature polymer electrolyte membrane fuel cell (HT PEM FC), but the surface conductance of this alloy is too low to be used as a bipolar. However, coating with a thin stable conductive layer, such as gold, will give suitable surface conductivity. Because the Hastelloy C22 is inert to corrosion, defect in the gold coating will not grow, and a gold-coated Hastelloy C22 bipolar plate should be suitable for use in a HT PEM fuel cell. Ongoing work concerns testing this assertion in HT PEM fuel cell stacks.

Open Access This article is distributed under the terms of the Creative Commons Attribution Noncommercial License which permits any noncommercial use, distribution, and reproduction in any medium, provided the original author(s) and source are credited.

References

1. D. Gervasio, J. Kinder, N. Hoskins, V. Onyeabor, S. Taghavi, A.V. Pattekar, K. Fleckner, High temperature polymer electrolyte membrane fuel cells (HT-PEMFCs) for portable power, Paper number 2006-01-3096, Power Systems Conference, Fuel Cells (Session Code: PSC6), Organizers—Michael Allen, Naval Air Systems Command; Nathan Kumbar, NAVAIR, New Orleans (2006)
2. K. Jayakumer, S. Pandiyan, N. Rajakshmi, K.S. Dhathathreyan, Cost-benefit analysis of commercial bipolar plates for PEMFC's. *J. Power Sources* **161**, 454–459 (2006)
3. J.J. Gray, C.A. Orme, Electrochemical impedance spectroscopy study of the passive films of alloy 22 in low pH nitrate and chloride environments. *Electrochim. Acta* **52**, 2370–2375 (2007)
4. S.P. Rogers, D.F. Gervasio, Oxygen electro-reduction on C22 and C276 nickel metal alloy. *Electrochem. Soc. Trans.* **3**, 431–442 (2006)
5. R.F. Silva, D. Franchi, A. Leone, L. Pilloni, A. Masci, A. Pozio, Surface conductivity and stability of metallic bipolar plate materials for polymer electrolyte fuel cells. *Electrochim. Acta* **51**, 3592–3598 (2006)
6. A. Pozi, F. Zaza, A. Masci, R.F. Silva, Bipolar plate materials for PEMFCs: a conductivity and stability study. *J. Power Sources* **179**, 631–639 (2008)
7. N. Priyantha, P. Jayaweera, D.D. MacDonald, A. Sun, An electrochemical impedance study of Alloy 22 in NaCl brine at elevated temperature. I. Corrosion behavior. *J. Electroanal. Chem.* **572**, 409–419 (2004)
8. D.D. Macdonald, A. Sun, N. Priyantha, P. Jayaweera, An electrochemical impedance study of Alloy-22 in NaCl brine at elevated temperature: II. Reaction mechanism analysis. *J. Electrochem. Chem.* **572**, 421–431 (2004)
9. M. Da Belo, N.E. Hakiki, M.G.S. Ferreira, Semiconducting properties of passive films formed on nickel–base alloys type Alloy 600: influence of the alloying elements. *Electrochim. Acta* **44**, 2473–2481 (1999)
10. M. Bojinov, G. Fabricius, P. Kinnunen, T. Laitinen, K. Mäkelä, T. Saario, G. Sundholm, Electrochemical study of the passive behaviour of Ni-Cr alloys in a borate solution—a mixed-conduction model approach. *J. Electroanal. Chem.* **504**, 29–44 (2001)